ELSEVIER

Journal of Molecular Catalysis A: Chemical 117 (1997) 229–242

JOURNAL OF MOLECULAR CATALYSIS A: CHEMICAL

# How do electronegative substituents make metal complexes better catalysts for the oxidation of hydrocarbons by dioxygen?

Arnd Böttcher, Eva R. Birnbaum, Michael W. Day, Harry B. Gray, Mark W. Grinstaff, Jay A. Labinger *

*Arthur Amos Noyes Laboratory, California Institute of Technology, Pasadena, CA 91125, USA*

Received 16 June 1996; accepted 17 July 1996

**Abstract**

Modeling studies support a radical-chain autoxidation mechanism for the aerobic oxidation of isobutane catalyzed by halogenated porphyrin iron complexes. A key role of the electronegative halogen substituents is to increase the $Fe^{III}/^{II}$ redox potential and thereby accelerate oxidation of the intermediate *t*-butyl hydroperoxide by (porph)$Fe^{III}$. The electronic structures of electronegatively substituted salen iron complexes have been characterized by several techniques, and related to changes in catalytic activity for oxidation of cyclohexene. The crystal and molecular structure of [Fe($(NO_2)_4$salen)($H_2O$)Cl] is reported.

*Keywords:* Hydrocarbon oxidation; Metalloporphyrins; Salen complexes

## 1. Introduction

With cytochrome P-450 as the exemplar, great efforts have been devoted to the study of metalloporphyrin complexes as catalysts for hydrocarbon oxidation [1], with particular recent emphasis on porphyrins containing some number of halogens or other electronegative substituents. Rationales include retarding oxidative degradation of the porphyrin, sterically blocking deactivating formation of $\mu$-oxo dimers, and activating potentially reactive metal–oxo intermediates by effectively destabilizing higher oxidation states relative to lower ones. The culmination of this approach in the fully halogenated porphyrins introduced by Lyons and Ellis [2,3] has produced remarkably efficient catalysts for oxidation of isobutane to *t*-butanol by $O_2$, in contrast to the vast majority of metalloporphyrin catalysts which require expensive oxo atom transfer oxidants, and afford lower activity, selectivity and stability.

We are examining the mechanisms of these and related catalytic reactions, the effects of electronegative substitution on structural, electronic, chemical and electrochemical properties of the complexes, the key factors that govern catalytic performance, and possibilities for developing later-generation catalysts for practical

* Corresponding author. Tel.: +1-818-3956520; fax: +1-818-4494159; e-mail: jal@cco.caltech.edu.


*PII* S1381-1169(96)00299-3

hydrocarbon oxidations. Previously we have reported molecular structures of a number of perhalogenated metalloporphyrin complexes [4], as well as spectroscopic and catalytic properties [4,5]. Experimental work along with a computer modeling study led to the conclusion that isobutane oxidation proceeds via a radical chain autoxidation mechanism, as presented in a preliminary communication [6]. We also introduced a new class of electronegatively substituted complexes, based on the salen ligand, and demonstrated that some members of that class exhibit *apparently* similar catalytic behavior, although certain anomalies raise questions about the degree of similarity [7].

In the present paper we report on our modeling work in fuller detail, extending its use for extrapolation and prediction; on characterization of the electronic structures of the salen-based catalysts, including the X-ray crystallographic structure of one example; and on the implications of these findings for mechanistic understanding and future prospects.

## 2. Results and discussion

### 2.1. Modeling metalloporphyrin-catalyzed isobutane oxidation

Mechanistic proposals for hydrocarbon oxidation catalyzed by metal complexes may be divided into two classes: (1) mechanisms involving metal-centered oxidants (M=O, MOOR, M(HOOR), etc.) that are directly responsible for C–H bond cleavage, and (2) mechanisms in which C–H bond cleavage is effected by metal-free species ($HO^{\cdot}$, $RO^{\cdot}$, $ROO^{\cdot}$, etc.) and the role of the catalyst is limited to promoting generation of the latter active species. Even this rather coarse-grained question is not so easy to answer for any given case (see, for example, Ref. [8]). A class (1) mechanism was originally proposed for oxidation of isobutane by Fe(TFPP)Cl and Fe(TFPPBr$_8$)Cl (Scheme 1) [2,3]. In this scheme (porph)$Fe^{IV}$=O is the active species. However, several experimental observations, most notably that the reduced (porph)$Fe^{II}$ reacts with $O_2$ only very slowly under conditions where catalysis is rapid [9], appear to make this proposal untenable.

$$Fe^{II} + O_2 \longrightarrow Fe^{II}\text{-}O\text{-}O$$
$$Fe^{II}\text{-}O\text{-}O + Fe^{II} \longrightarrow Fe^{III}\text{-}O\text{-}O\text{-}Fe^{III}$$
$$Fe^{III}\text{-}O\text{-}O\text{-}Fe^{III} \longrightarrow 2\ Fe^{IV}{=}O$$
$$Fe^{IV}{=}O + RH \longrightarrow Fe^{III}\text{-}OH + R^{\cdot} \longrightarrow Fe^{II} + ROH$$
$$Fe^{IV}{=}O + Fe^{II} \rightleftharpoons Fe^{III}\text{-}O\text{-}Fe^{III}$$

For a class (2) mechanism to account for high activity even at ambient temperatures, the catalytic steps (Eqs. (7) and (7a) in Scheme 2) would have to be unusually rapid. In fact, Fe(TFPPBr$_8$)Cl *is* an extraordinarily active catalyst for decomposition of *t*-butyl hydroperoxide [4,10]. According to this view, halogenation of the porphyrin ring indeed stabilizes lower oxidation states, but the consequence in terms of catalytic activity is not to make an Fe=O species more oxidizing towards a C–H

$$RH \xrightarrow{k_i} R^{\cdot} \xrightarrow{O_2,\ fast} ROO^{\cdot} \quad \text{(i)}$$

$$ROO^{\cdot} + RH \xrightarrow{k_1} ROOH + R^{\cdot} \xrightarrow{O_2,\ fast} ROO^{\cdot} \quad \text{(1)}$$

$$2\ ROO^{\cdot} \xrightarrow{k_2} 2\ RO^{\cdot} + O_2 \quad \text{(2)}$$

$$2\ ROO^{\cdot} \xrightarrow{k_3} ROOR + O_2 \quad \text{(3)}$$

$$RO^{\cdot} + RH \xrightarrow{k_4} ROH + R^{\cdot} \xrightarrow{O_2,\ fast} ROO^{\cdot} \quad \text{(4)}$$

$$RO^{\cdot} + ROOH \xrightarrow{k_5} ROH + ROO^{\cdot} \quad \text{(5)}$$

$$RO^{\cdot} \xrightarrow{k_6} Me_2C{=}O + Me^{\cdot} \xrightarrow{O_2,\ fast} MeOO^{\cdot} \quad \text{(6)}$$

$$MeOO^{\cdot} + ROO^{\cdot} \xrightarrow{fast} ROH + CH_2O + O_2 \quad \text{(6a)}$$

$$ROOH + M^{III} \xrightarrow{k_c} ROO^{\cdot} + H^{+} + M^{II} \quad \text{(7)}$$

$$ROOH + M^{II} \xrightarrow{fast} RO^{\cdot} + OH^{-} + M^{III} \quad \text{(7a)}$$

Scheme 2.

bond, as in Scheme 1, but rather to accelerate the slower of the two catalytic steps, the oxidation of ROOH by (porph)$Fe^{III}$. In accord with this picture, the activity for peroxide decomposition correlates directly with redox potential [10].

Though high peroxide decomposition activity is *necessary* to account for a class (2) radical chain autoxidation mechanism for isobutane oxidation, is it also *sufficient*? That question may be addressed by computer modeling, as rate constants for steps not involving catalytic species are available from the literature, and $k_c$ should be obtainable from the peroxide decomposition data. Although Scheme 2 is oversimplified, neglecting a number of alternate reactions (e.g., abstraction by radicals of primary C–H bonds), only traces of products from such reactions are typically detected, and this limited set should be adequate for our purposes. With only one additional simplifying assumption — that the sole fate of the methylperoxy radical produced in Eq. (6) is termination according to Eq. (6a) — we gain a major advantage of convenience. The set of differential equations derived from the reaction set of Scheme 2, which without these assumptions would constitute stiffly coupled equations requiring a relatively elaborate computer program for solution, can be algebraically transformed into a non-stiffly coupled set that can be solved by a simple desktop computer-BASIC level program using the Euler method. (The algebra, the final differential equations, and the literature-derived rate constants were all presented in the preliminary communication [6] and are not reproduced here.)

Table 1 shows the results of modeling just the peroxide decomposition, using $k_c$ as an adjustable variable to fit the experimental data [10]. It may be noted that it was also necessary to treat $k_6$, the rate constant for dissociation of *t*-BuO$^{\cdot}$ into Me$^{\cdot}$ plus acetone, as adjustable, since the literature value ($8 \times 10^2$ to $3 \times 10^3$ $s^{-1}$) consistently gave predictions of acetone yield far below the observed values, no matter how the remaining parameters were varied.

Table 1
Calculated and observed decomposition of *t*-butyl hydroperoxide by three (porph)$Fe^{III}$ complexes

| | (TPP)FeCl | | (TFPP)FeCl | | (TFPPBr$_8$)FeCl | |
|---|---|---|---|---|---|---|
| | expt. | model | expt. | model | expt. | model |
| $k_c$ ($M^{-1}$ $s^{-1}$) | | 0.6 | | 1.1 | | 4.7 |
| $k_6$ ($s^{-1}$) | | $1 \times 10^6$ | | $2 \times 10^5$ | | $8 \times 10^4$ |
| Time (h) | 1.9 | 1.9 | 3.3 | 3.3 | 1.9 | 1.9 |
| Conversion (%) | 27 | 25 | 72 | 72 | 95 | 95 |
| ROH (%) | 82 | 85 | 87 | 89 | 90 | 90 |
| $Me_2C{=}O$ (%) | 11 | 7 | 3 | 3 | 2 | 2 |
| ROOR (%) | 7 | 8 | 10 | 8 | 8 | 8 |

There is in fact precedent for the fact that that reaction *can* be catalyzed by metal complexes [11]; whether an overall acceleration of 2–3 orders of magnitude, or a range among the three catalysts tested of more than an order of magnitude, are reasonable expectations may be open to some question. However, the values used do give good agreement for selectivities to various products, as shown in Table 1, while the derived values for $k_c$ show the same (logarithmic) correlation with redox potential (Fig. 1) that was found for the raw activity data.

The next step is to model the actual isobutane oxidation data, keeping the values for $k_6$ and $k_c$ now fixed and not adjustable. An additional adjustable parameter, the initiation rate $k_i$, must

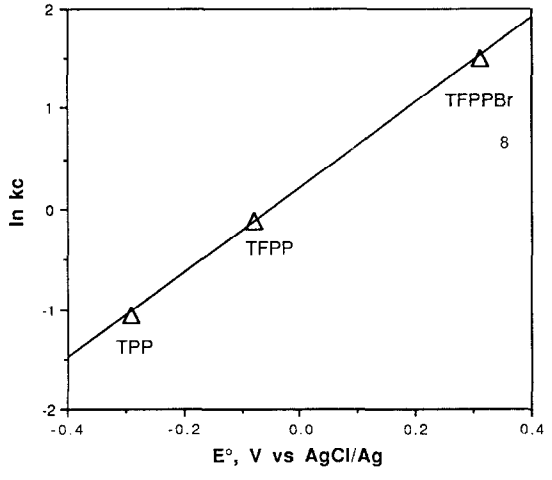


Fig. 1. Correlation of *t*-butyl hydroperoxide decomposition activity (as measured by $k_c$ value calculated from model) with $Fe^{III/II}$ redox potential.

be introduced; intuitively one might expect that its value would be crucial. However, that turns out not to be the case, at least within the framework of the approximate model used: the calculated degree of conversion is *insensitive* to the value of $k_i$ over a wide range. Qualitatively, this is because Eqs. (7) and (7a) now become by far the major source of radicals, and there is no very efficient chain-termination step. The value selected for $k_i$ begins to have an impact on calculated results only when it is set sufficiently high that the model predicts significant conversion in the absence of any catalyst ($k_c = 0$). A value of $k_i = 10^{-10}$ $s^{-1}$ was used, based on extrapolations from high-temperature uncatalyzed autoxidation; this value predicts $< 0.2\%$ conversion without catalyst at 25°.

The results of calculations under the above constraints are shown in Table 2, along with comparative experimental data [3]. The agreement between predicted and observed activity for the two active catalysts is striking. For $(TFPPBr_8)FeCl$ the model predicts a significant yield of di-*t*-butyl peroxide, which was not detected in the original experimental report. However, a more recent reexamination of this system reported that the latter product *is* indeed formed, in approximately the amounts predicted (conditions of those experiments were not completely identical to those modeled) [12]. Thus, for the most active catalyst, the model accurately predicts both activity and selectivity, and hence the autoxidation mechanism of Scheme 2 accounts fully for the isobutane oxidation activity.

Two other anomalies appear in Table 2. For the $(TFPP)Fe^{III}$ catalyst (the role, or lack thereof, of the axial ligand is discussed below), the model predicts lower overall ROH selectivity and higher acetone yield than observed. This is presumably due to one or both of the following: the failure to detect ROOR which may actually have been present, as found for the perhalogenated catalyst, and the difficulty of choosing a reliable rate constant for the acetone-producing step, as discussed earlier. The other is the

Table 2
Calculated and observed oxidation of isobutane by three $(porph)Fe^{III}$ complexes

| | (TPP)FeCl | | (TFPP)FeOH | | $(TFPPBr_8)FeCl$ | |
|---|---|---|---|---|---|---|
| | expt. | model | expt. | model | expt. | model |
| Time (h) | any | 143 | 143 | 143 | 71.5 | 71.5 |
| Conversion (%) | — | 3.5 | 18 | 18 | 22 | 23 |
| ROH (%) | — | 62 | 95 | 77 | 91.5 | 85 |
| $Me_2C{=}O$ (%) | — | 35 | 5 | 16 | 8.5 | 8.5 |
| ROOH (%) | — | 1 | — | — | — | — |
| ROOR (%) | — | 2 | — | 6 | — | 7 |

prediction of small but significant activity for the baseline $(TPP)Fe^{III}$ catalyst, whereas none at all is observed.

To interpret the latter, let us first look at Fig. 2. Since we have a correlation between the value of $k_c$ and the redox potential, and since we can use $k_c$ to calculate overall isobutane oxidation activity for a hypothetical catalyst, we can combine these to predict a correlation between isobutane oxidation and redox potential; that is shown in Fig. 2. (For the purpose of this calculation the value of $k_6$ is held constant at that for $(TFPPBr_8)FeCl$ in Table 1.) Again, it is evident that the two active catalysts give good agreement, but $(TPP)Fe^{III}$ does not. However, note the potentials for the $\mu$-oxo dimers $((TPP)Fe)_2O$ and $((TFPP)Fe)_2O$, and the corre-

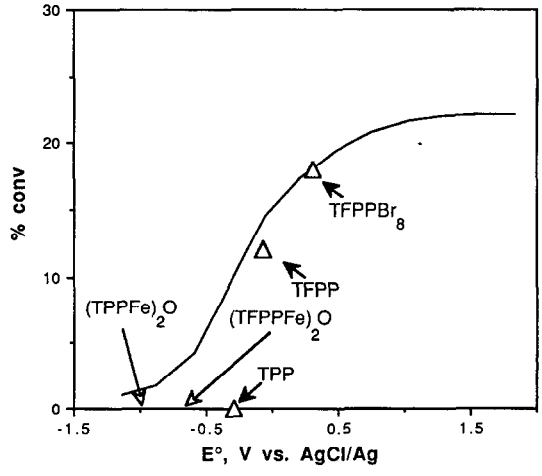


Fig. 2. Calculated isobutane oxidation activity as a function of $Fe^{III/II}$ redox potential (curve), experimental data (triangles), and redox potentials for $\mu$-oxo dimers (open arrows).

$$Fe^{III}\text{-}O\text{-}Fe^{III} + ROOH \longrightarrow Fe^{III}\text{-}OH + ROO\cdot + Fe^{II}$$
$$Fe^{II} + ROOH \longrightarrow Fe^{III}\text{-}OH + RO\cdot$$

Scheme 3.

sponding predicted activities. The former should be essentially inactive, while the latter should have some activity, albeit less than the corresponding monomer.

This observation suggests an interpretation of the experimental inertness of $(TPP)Fe^{III}$. $((TPP)Fe)_2O$ is well-known to form readily under oxidizing conditions, so even if the monomeric complex with this unhalogenated ligand had the catalytic activity predicted by the model, it would rapidly convert to the inactive form. Then why doesn't the $(TFPP)Fe^{III}$ complex also give the activity predicted for the dimer? Because the catalytic cycle will reconvert any dimer back to monomer, according to Scheme 3; and as long as that monomer turns over more rapidly than it dimerizes, the predominant form participating in catalysis will be the monomer. Spectroscopic studies have in fact shown that the monomer predominates in solution under catalytic conditions, although some dimer is also detectable [12]. (For the more sterically hindered $(TFPPBr_8)Fe^{III}$ system, we have not been able to see any evidence for dimerization.) Scheme 3 also explains why there is little dependence on axial ligand [2,3], since by passing through the (presumably) axial ligand-free $Fe^{II}$ state each time around the cycle, the active catalyst will rapidly be converted to a common form, probably the hydroxide as shown, no matter what is present at the outset of the reaction.

### 2.2. Extrapolation of modeling results

Let's consider two issues: improving catalytic activity for isobutane oxidation, and extending oxidation by this mechanism to other hydrocarbons. According to Fig. 1 we should be able to increase the peroxide decomposition activity at will by just making the complex more oxidizing. Presumably we can achieve that by adding more and/or better electron-withdrawing substituents. That assumes of course that redox potential is the only parameter of importance, which almost surely is not the case (see below). Also, we would expect to reach a point where the redox potential is so high that ROOH reduction (7a) would become slower than ROOH oxidation (7) and hence rate-determining. That should give us a maximum. However, Fig. 2 shows that we have relatively little to gain thereby. The increased peroxide decomposition rate translates into only a modest increase in isobutane oxidation, and the catalysts already examined are nearly at the plateau level already. Hence the model predicts there is in fact little room for improvement.

As for other (non-tertiary) C–H bond oxidations, there are two problems. First, the C–H bond will be stronger, so propagation steps (Eqs. (1) and (4) in Scheme 2) will be somewhat slower. Second, and more serious, termination is *much* faster, as the equivalent of Eq. (3) for a tertiary alkylhydroperoxide becomes instead Eq. (8) (illustrated for *i*-propyl hydroperoxide), with rate constants typically two or more orders of magnitude higher than $k_3$. As a consequence, the autoxidation mechanism cannot give efficient oxidation; chain lengths are very short, and selectivities are low. Calculations for oxidation of propane (necessarily highly approximate, as rate constants need to be corrected for temperature differences and other changes) suggest that conversions will only be on the order of $< 1\%$ at around 125°, no matter how high we make the value of $k_c$. This is pretty much in agreement with observations [2,3].

$$2(CH_3)_2CHOO\cdot \rightarrow (CH_3)_2CHOH + (CH_3)_2C{=}O + O_2 \quad (8)$$

### 2.3. Electronic structural characterization of electronegatively substituted salen complexes

In spite of their good activity for aerobic isobutane oxidation, the metalloporphyrin catalysts have limited practical applicability because

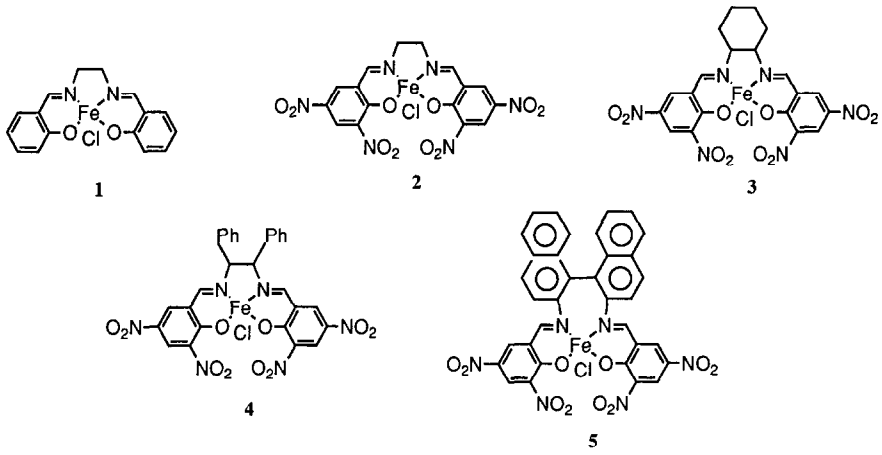


Fig. 3. Iron salen derivatives **1–5**.

of the difficulty and cost of their preparation. Since modeling, as discussed above, indicates that increases in activity sufficient to overcome these drawbacks are unlikely, a more promising approach would be to make an equally active but much cheaper catalyst. The non-macrocyclic tetradentate ligand salen (**1**) is often used as a porphyrin surrogate; but modified salen complexes are much more readily accessible than most porphyrins.

We have previously reported the synthesis of a series of electronegatively substituted iron salen complexes, along with their activity for catalytic aerobic oxidation of cyclohexene at room temperature [7]. Some of the complexes studied are depicted in Fig. 3, and their oxidation activities (along with comparison data for the porphyrin complexes studied in the previous section) are summarized in Fig. 4. The product selectivities, and sensitivity to the addition of radical chain initiators or inhibitors, are very similar for the porphyrin and salen catalysts [7].

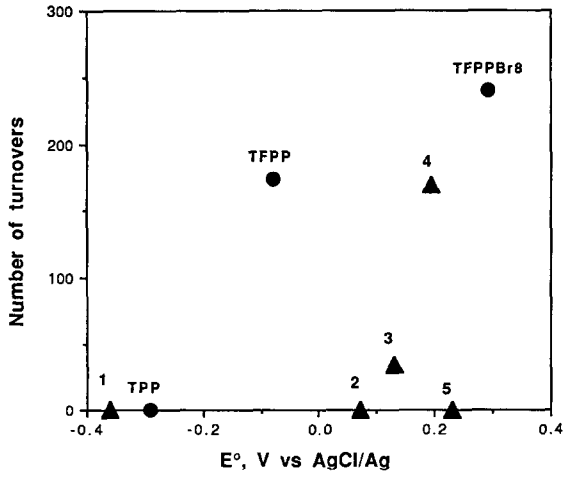


Fig. 4. Cyclohexene oxidation activity as a function of $Fe^{III/II}$ redox potential for iron porphyrin (circles) and salen (triangles) complexes.

It can be seen that redox potential for the salen derivatives can be systematically varied by substitution, and the activity–potential relationship is qualitatively similar to that found for porphyrin complexes. In fact, some of the more strongly oxidizing complexes catalyze aerobic oxidation with activity approaching that of the better porphyrin catalysts. However, the activity–potential relationship is not *quantitatively* the same for the two classes of complex: a salen-based catalyst needs a redox potential around 300 mV higher than the porphyrin catalyst of comparable activity. Also, there is a striking reversal in the salen data: the most oxidizing complex, **5**, is completely inactive, while the next most oxidizing, **4**, is the most active.

How are these anomalies to be interpreted? Assuming that the mechanism is fundamentally the same as that established above, the only role

of the catalyst is to decompose alkyl hydroperoxide intermediates. If those reactions do not correlate simply with potential, then they must involve *inner-sphere* oxidation/reduction of peroxide by catalyst, wherein the activity depends not only on the redox potential but also on the specific interaction between the peroxide and the metal center and the energetics of structural reorganization during reaction. Accordingly, detailed investigations of molecular and electronic structure are needed to resolve these issues.

The electronic structure of the parent salen complex [Fe(salen)Cl] (**1**) is typical of high-spin $Fe^{III}$. Most characteristic is the solution $^1H$ NMR spectrum, which reveals (among other features) two signals, paramagnetically shifted to low field at around $\delta$ 40 and 70, corresponding to the 4- and 6-protons of the phenyl rings [13]. These positions remain unsubstituted in all the derivatives we have prepared. All of them, *with the exception of inactive complex* **5**, show the same pattern; in contrast **5** has no peaks with such large paramagnetic shifts, but does exhibit sharp peaks in the normal region for aromatic protons (Fig. 5). UV–visible spectra behave analogously: the spectra for **1–4** are very similar to one another, but that for **5** is quite different (Fig. 6).

Magnetic moments, measured by SQUID in the solid state, are complicated by the possibility of partial aggregation. The parent complex [Fe(salen)Cl] is known to exist both in a dimeric, hexacoordinate as well as in a monomeric, pentacoordinate structure in the solid state, depending on the solvent system and the conditions used for crystallization, whereas it is monomeric in solution [14–16]. In the dinuclear complex

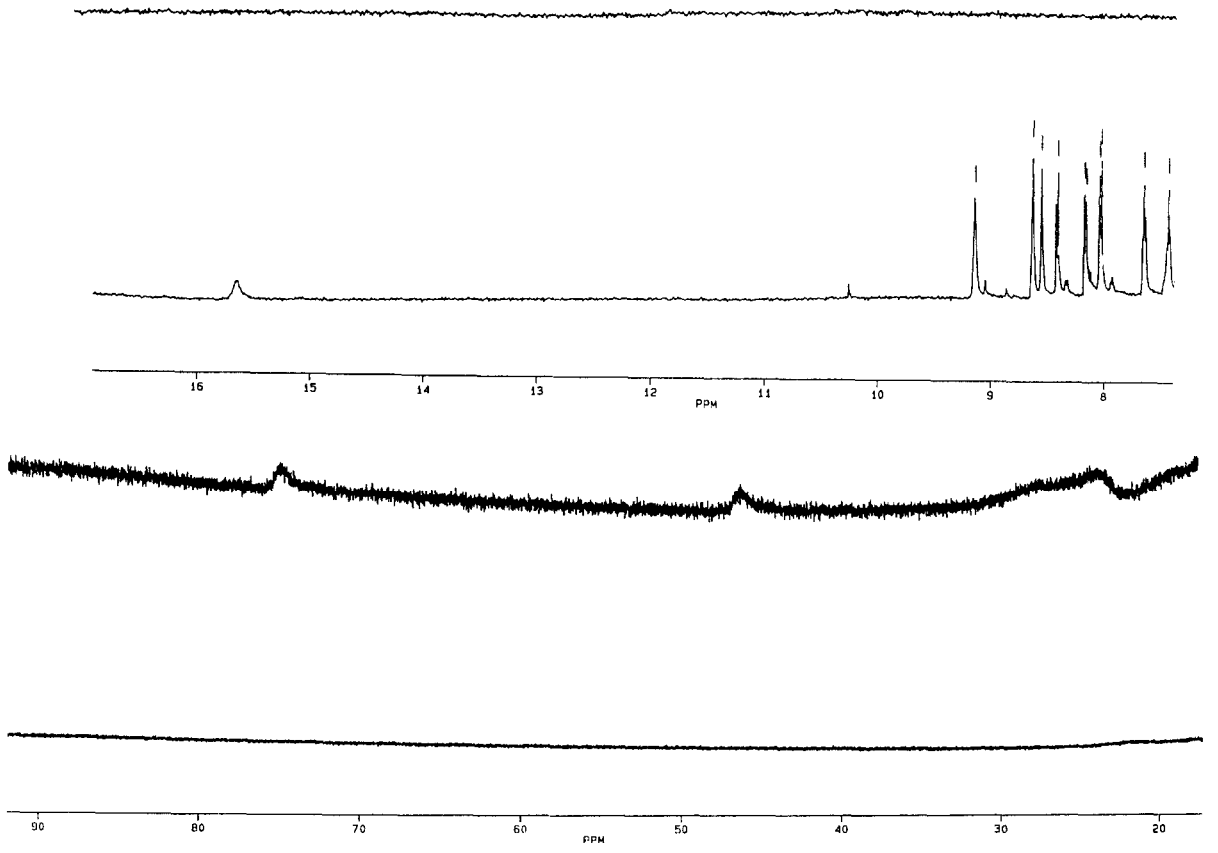


Fig. 5. NMR spectra of complexes **2** (upper traces) and **5** (lower traces).

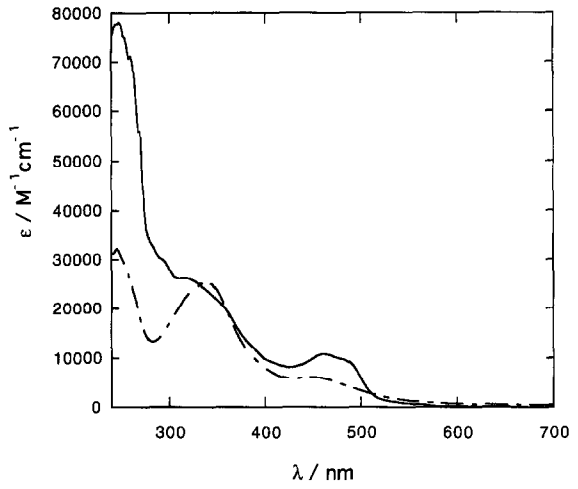


Fig. 6. UV–visible spectra of complexes **2** (dotted line; the spectra of **1**, **3** and **4** are very similar) and **5** (solid line).

$[Fe(salen)Cl]_2$ dimerization is achieved by sharing of one oxygen atom from each salen ligand by two iron atoms. This bridging interaction results in some magnetic coupling; thus the parent [Fe(salen)Cl] has a magnetic moment of 5.4 [17], considerably reduced from the spin-only value of 5.9. Table 3 shows magnetic moments as well as other data for the complexes; the magnetic moment for **5** is significantly lower than that for any of the others. Combining this with the NMR and UV–visible spectral data, it seems clear that **5** has a different electronic structure, probably an intermediate spin state, whereas **1–4** are all apparently normal high-spin $Fe^{III}$ in solution.

Table 3
Parameters for [Fe(salen)Cl] derivatives

| Complex | $E^\circ$ (V) (versus AgCl/Ag) | Activity | Magnetic moment [a] | Hi-spin NMR [b] |
|---|---|---|---|---|
| **1** | −0.36 | 0 | 5.4 | yes |
| **2** | 0.07 | 0 | 5.9 | yes |
| **3** | 0.13 | medium | 5.3 | yes |
| **4** | 0.195 | high | 4.7 | yes |
| **5** | 0.23 | 0 | 3.8 | no |

[a] Solid-state, 300 K.
[b] Exhibits characteristic peaks at $\delta \sim 40$, $\sim 70$.

## 2.4. Molecular structure of $[Fe((NO_2)_4salen)(H_2O)Cl]$ (2)

We have tried to obtain crystals suitable for X-ray analysis for these new complexes, especially **4** and **5**, but so far have succeeded only for **2**. Fig. 7 shows a view of the molecular structure of $[Fe((NO_2)_4salen)(H_2O)Cl]$ with the atomic labeling scheme. The complex is monomeric in the solid state, with distorted octahedral geometry around the iron center. The tetradentate Schiff base ligand ($N_2O_2$ donor set) coordinates the iron atom in the equatorial plane with aquo and chloro ligands occupying the axial positions of the complex. (The compound also crystallizes with one nitromethane molecule, which is not coordinated.) Presumably the electron-withdrawing nitro substituents make the iron center in **2** more Lewis acidic, stabilizing the six-coordinate form relative to **1**,

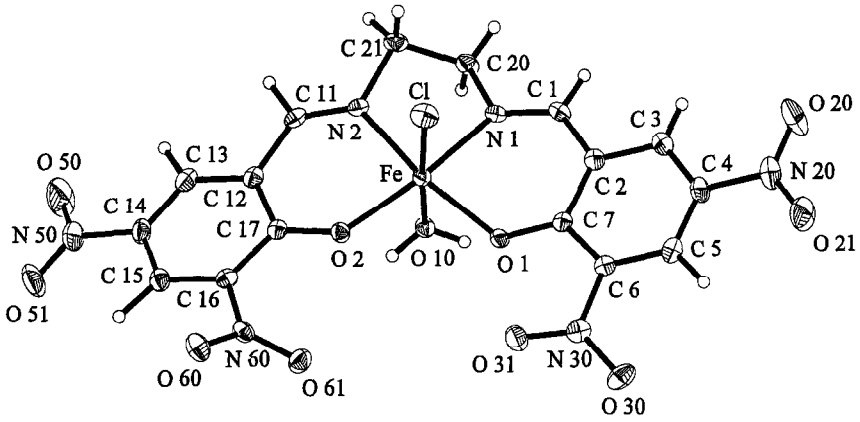


Fig. 7. X-ray crystal structure (plot with 50% probability ellipsoids) of $[Fe((NO_2)_4salen)(H_2O)Cl]$ showing the atomic labeling scheme.

Table 4
Selected bond distances (Å) and bond angles (°) in [Fe($(NO_2)_4$salen)($H_2O$)Cl]

| Bond [a] | |
|---|---|
| Fe–N(1) | 2.101(2) |
| Fe–N(2) | 2.087(2) |
| Fe–Cl | 2.2638(7) |
| Fe–O(1) | 1.976(2) |
| Fe–O(2) | 1.9571(14) |
| Fe–O(10) | 2.137(2) |
| **Angle [a]** | |
| N(1)–Fe–N(2) | 79.41(7) |
| O(1)–Fe–N(1) | 85.87(6) |
| O(1)–Fe–O(2) | 103.52(6) |
| O(2)–Fe–N(2) | 88.62(6) |
| N(1)–Fe–Cl | 93.49(5) |
| N(2)–Fe–Cl | 96.25(5) |
| O(2)–Fe–O(10) | 86.20(7) |
| O(1)–Fe–O(10) | 84.71(6) |
| O(10)–Fe–Cl | 175.13(5) |
| O(2)–Fe–N(1) | 163.92(6) |
| O(1)–Fe–N(2) | 161.71(6) |

[a] See Fig. 7 for atomic numbering.

which as noted above is either monomeric five-coordinate or dimeric in the solid state.

Selected bond lengths and angles are listed in Table 4. The structural details are similar to those previously found for related complexes. The octahedral coordination about the iron is significantly distorted: the O–Fe–N angles in the equatorial plane (85.87(6)° and 88.62(6)°) are close to 90°, whereas the N–Fe–N angle (79.41(7)°) is relatively small, and the O–Fe–O angle (103.52°) is much larger. This pattern is typical for octahedral iron salen complexes: O–Fe–O angles between 100.5 and 108.7° have been observed [16,18,19], whereas only the pentacoordinate iron salen complex [Fe(salen)Cl] shows a much smaller O–Fe–O angle (93.9°) [14]. The distance between the iron atom and the chloro axial ligand is 2.2638(7) Å and lies within the range found for the Fe–Cl distances in related complexes, e.g. [Fe(salen)Cl] (2.238(4) Å) [14] and [Fe(salen)Cl]$_2$ (2.294(3) Å) [16].

The Fe–O and Fe–N bond lengths in the equatorial ligand plane of **2** are 1.976(2) Å and 1.9571 (14) Å (Fe–O), and 2.101(2) Å and 2.087(2) Å (Fe–N), respectively. These Fe–N bond distances (average value = 2.094 Å) are about the same as for [Fe(salen)Cl] (2.082 Å [14] or the corresponding dimer [Fe(salen)Cl]$_2$ (2.095 Å) [16]. Two related monomeric complexes with octahedral coordination, [Fe(salen)(Im)$_2$]$ClO_4$ (Im = imidazole) [19] and [Fe(3-MeO-salen)(5-Ph–Im)($H_2O$)]$BPh_4$ (Ph = phenyl, MeO = methoxy) [18], have average Fe–N distances of 2.118 and 2.071 Å, respectively. In contrast, the average Fe–O bond length for six-coordinate **2** (1.967 Å) is significantly longer than that for five-coordinate [Fe(salen)Cl] (1.882 Å), but not for the dimer [Fe(salen)Cl]$_2$ (1.938 Å). This suggests that the presence or absence of a sixth axial ligand has the largest effect on metal–salen bonding, and that the effect is manifested much more significantly in the Fe–O than the Fe–N bond lengths. (However, the average Fe–O distances for both [Fe(salen)(Im)$_2$]$ClO_4$ (1.917 Å) and [Fe(3-MeO-salen)(5-Ph–Im)($H_2O$)]$BPh_4$ (1.886 Å) are shorter than those of [Fe($(NO_2)_4$salen)($H_2O$)Cl].) The distance between the Fe atom and the aquo ligand is significantly greater in [Fe(3-MeO-salen)(5-Ph–Im)($H_2O$)]$BPh_4$ (2.205(4) Å) than in [Fe($(NO_2)_4$salen)($H_2O$)Cl] (2.137(2) Å).

From the point of view of catalysis, the most interesting structural question may be the distortion of the tetradentate ligand. Catalytically active perhalogenated iron porphyrins are distorted in two regards: the four nitrogen donor atoms are displaced relative to their mean plane to give some degree of tetrahedral distortion, and the porphyrin ligand backbones exhibit considerable distortion from planarity ('saddling' and 'ruffling') [4,20]. The chelate ligands in iron salen complexes also typically exhibit non-planar ligand conformations, usually either 'umbrella' or 'stepped' (for a definition and schematic structures, see Ref. [21]). The structure of **2** shows a 'stepped' conformation with one of the benzene rings bent slightly upward by 19.27° and the other bent slightly downward by 17.96° with respect to the least squares plane defined by the $N_2O_2$ donor atoms (see the side

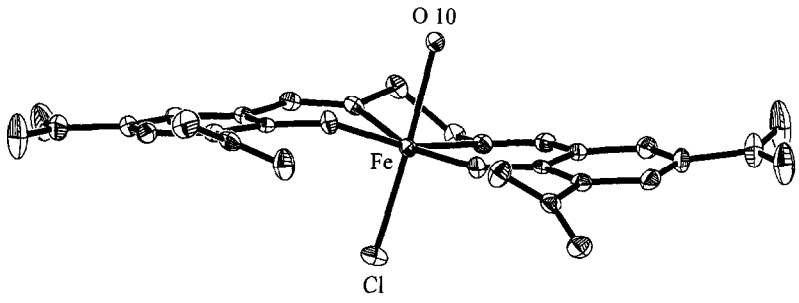


Fig. 8. 'Side view' of $[Fe((NO_2)_4salen)(H_2O)Cl]$.

view in Fig. 8). The dimeric complex $[Fe(salen)Cl]_2$ also has a 'stepped' arrangement, whereas most other known iron salen complexes, including the monomer [Fe(salen)Cl], prefer an 'umbrella' conformation [22].

In $[Fe((NO_2)_4salen)(H_2O)Cl]$ the iron atom is displaced by 0.213(1) Å from the $N_2O_2$ plane, an intermediate value compared to related iron salen complexes: typical displacements range from 0.005 to 0.57 Å. However, complex **2** shows almost *no* tetrahedral distortion of the $N_2O_2$ plane, as measured by the NOON dihedral angle of 0.23(6)°. In other iron salen complexes torsion angles of up to 15° have been observed [22].

## 3. Conclusions

The modeling studies described here fully support the proposal, that aerobic oxidation of isobutane catalyzed by halogenated porphyrin iron complexes follows a 'traditional' radical-chain mechanism. We cannot rule out the possibility that oxidation by metal–oxo species might also participate to some degree, perhaps as an initiation mechanism, but the experimental observations appear to be fully accounted for without postulating any such additional processes. The extraordinary catalytic activity even at room temperature is a consequence of the electronegative halogen substituents on the porphyrin ring, which exert their effect in (at least) the following three ways: replacing the C–H bonds which make most metalloporphyrins susceptible to oxidative degradation (though it should be noted that more recent studies [12] indicate that these catalysts are not as stable as previously reported [2,3]), providing steric hindrance to deactivation by $\mu$-oxo dimer formation (see below for another possible role for steric factors), and most importantly by increasing the $Fe^{III/II}$ redox potential and thereby increasing the rate of oxidation of *t*-butyl hydroperoxide, the rate-determining step of the catalytic part of the mechanism.

Extrapolation of the modeling results implies two further predictions: that continuing to increase the redox potential will not translate into a large acceleration of isobutane catalytic activity, and that these catalysts will not be very effective for selective aerobic hydroxylation of non-tertiary C–H bonds by this mechanism.

The same approach — increasing electronegative substitution — succeeds in generating oxidation catalysts from the more readily accessible salen class of complex. However, the correlation of activity with redox potential is not so smooth as with the porphyrins — the most oxidizing complex so far studied is catalytically inactive — and higher potentials are required for comparable activity. We tentatively explain both these anomalies in terms of the detailed, inner-sphere electron-transfer mechanism for ROOH oxidation. The inactive salen complex has a different electronic structure from those that are active. While neither the exact nature of its electronic structure nor its cause has been established, we expect that the spin-state change will have a significant impact on the ability of the complex to undergo ligand substitution and coordination of ROOH, and consequently on the oxidation rate.

As for the differences in required potential between the two classes of complex, we note the substantial tetrahedral distortion in the active porphyrin complexes (resulting at least in part from the steric bulk of the halogen substituents), and the lack of any such distortion in the one (inactive) salen complex we have thus far been able to crystallize. We suggest that distortions may be connected to catalytic activity as follows: if the crucial step for catalytic activity is oxidation of ROOH by (ligand)$Fe^{III}$, as suggested by the mechanistic study of porphyrin complexes, then distortion of the *ground-state* structure may lower the reorganization energy, and thus the overall activation energy for the electron-transfer reaction. The apparent shift to higher potentials required for the salen complexes, compared to the metalloporphyrins, might thus reflect the 'boost' provided by the greater distortion of the latter. Unfortunately no crystal structure of a catalytically active iron salen complex (**3** or **4**) has yet been obtained.

Before closing, we should consider the possibility that the mechanism of cyclohexene oxidation by iron salen complexes is in fact *not* the same as that established for isobutane oxidation by iron porphyrin complexes. As noted earlier, all the hallmarks such as product distribution, susceptibility to inhibition, etc., are similar. However, the salen complexes are not very active for *t*-butyl hydroperoxide decomposition. That may indicate that the mechanism of Scheme 2 is not operating, or that catalytic decomposition of cyclohexenyl hydroperoxide is much faster with these complexes. This issue, along with the structural questions raised above, remain to be tested.

## 4. Experimental

All experimental details for synthesis and catalytic testing of iron salen complexes have been published previously [7]. NMR spectra were recorded on a Bruker AM 500 instrument ($CH_3CN$ solutions); UV–visible spectra, on a HP 8452A spectrometer ($CH_2Cl_2$ solutions). Magnetic susceptibilities were determined using a Quantum Design SQUID magnetometer.

Red crystals of [Fe($(NO_2)_4$salen)($H_2O$)Cl] suitable for X-ray crystallography were grown at room temperature by slow evaporation from a nitromethane/ethanol solution containing ca. 5% $H_2O$. Cell dimensions and intensity data were measured with an Enraf-Nonius CAD-4 diffractometer at 160 K using monochromated Mo K$\alpha$ radiation. Cell dimensions were determined by least-squares refinement of 25 reflections with $2\theta$ angles from 11.5–12.1°. Three control reflections measured every 60 min

Table 5
Crystallographic data for [Fe($(NO_2)_4$salen)($H_2O$)Cl]

| | |
|---|---|
| Formula | $C_{17}H_{15}ClFeN_7O_{13}$ |
| Molecular weight | 616.66 |
| Color | red |
| Shape | irregular |
| Crystal system | monoclinic |
| Space group | P $2_1/c$ (# 14) |
| $a$ (Å) | 11.483(2) |
| $b$ (Å) | 17.831(4) |
| $c$ (Å) | 11.678(2) |
| $\beta$ (deg) | 100.15(3) |
| $V$ (Å$^3$) | 2353.7(8) |
| $Z$ | 4 |
| $D_x$ (g cm$^{-3}$) | 1.74 |
| Radiation | Mo K$\alpha$ |
| Wavelength (Å) | 0.71073 |
| $\mu$ (cm$^{-1}$) | 8.38 |
| Temperature (K) | 160 |
| Crystal size (mm) | 0.33×0.3×0.3 |
| Diffractometer | Enraf-Nonius CAD-4 |
| Collection method | omega scans |
| $\theta$ range (deg) | 2.0 to 25.0 |
| $h_{min/max}$ | −13/13 |
| $k_{min/max}$ | 0/21 |
| $l_{min/max}$ | −13/13 |
| Reflections collected | 8897 |
| Independent reflections | 4116 |
| Reflections used | 4116 |
| $F(000)$ | 1252 |
| $R_{int}$ | 0.019 |
| $R(F)$ | 0.031 |
| $R_w(F^2)$ | 0.073 |
| $(\Delta/\sigma)_{max}$ | −0.07 |
| Goodness of fit | 2.34 |

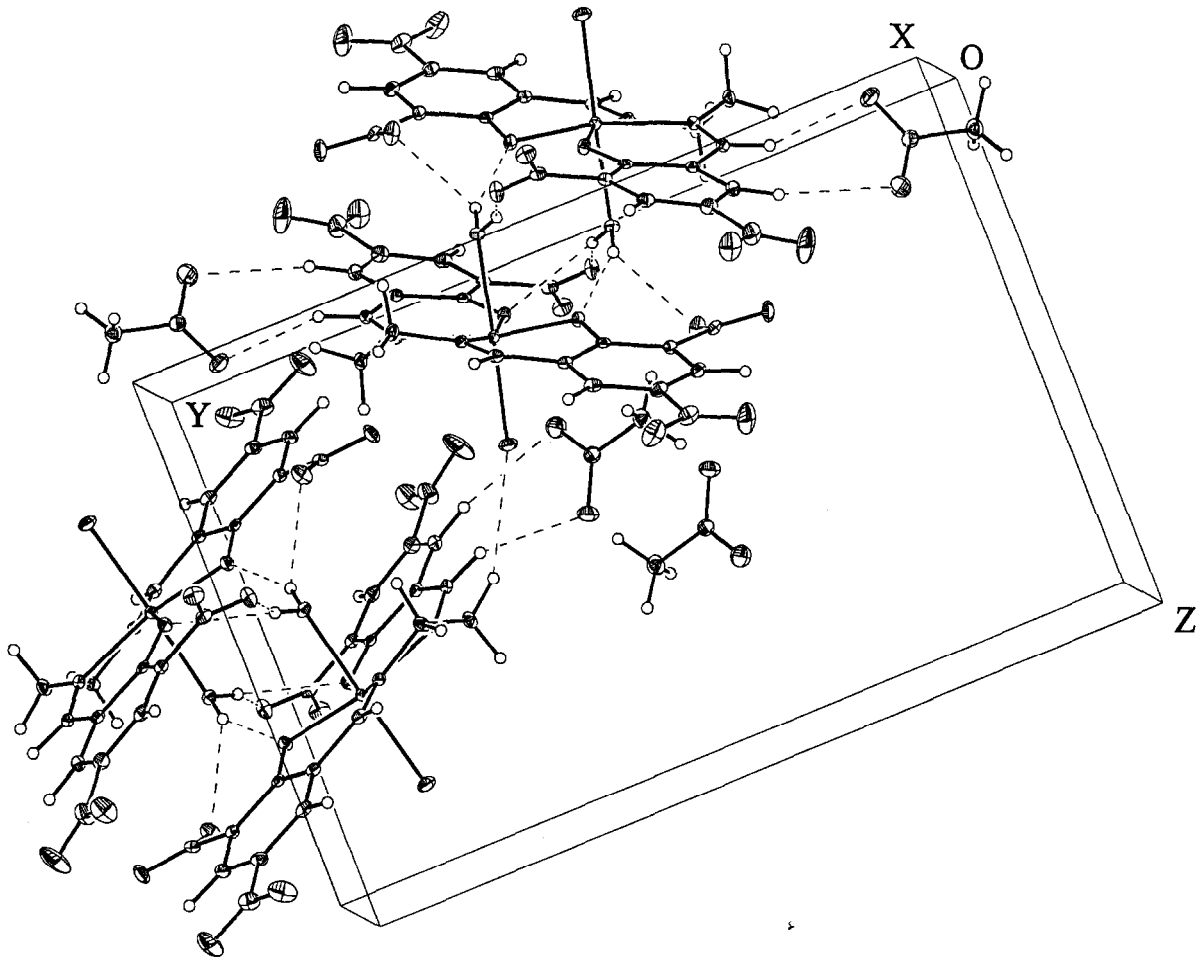


Fig. 9. Unit cell of [Fe($(NO_2)_4$salen)($H_2O$)Cl] (plot with 30% probability ellipsoids).

showed no loss of intensity during data collection. Lorentz and polarization corrections, but no absorption correction, were applied. Atom scattering factors were taken from Cromer and Waber [23] and Cromer [24]. CRYM [25], SHELXS-86 [26], SHELXL-93 [27] and XP/PC [28] programs were used. The structure was solved by direct methods using SHELXS-86 and refined using full matrix least-squares techniques. Hydrogen atoms were found by difference Fourier synthesis and freely refined. Final difference Fourier maps showed largest residuals of $+0.523$ and $-0.433$ e $Å^{-3}$. A summary of data collection and refinement is given in Table 5; unit cell parameters are given in Table 6.

Fig. 9 gives a view of the unit cell of [Fe($(NO_2)_4$salen)($H_2O$)Cl]. Shortest intermolecular contacts (weak hydrogen bonds) are involved between a hydrogen atom of the water molecule coordinated to the iron center and an oxygen atom of a nitro substituent of a neighboring complex molecule (2.057 Å) and between the other hydrogen atom of this water molecule and one chelating oxygen atom of the neighboring complex molecule (2.09 Å). The O–H–O bond angles are close to 180° and are thus in line with the assumption of weak inter-

Table 6
Atomic coordinates ($\times 10^4$) [a] and equivalent isotropic displacement parameters [b] ($\times 10^3$ Å$^2$) for [Fe((NO$_2$)$_4$salen)(H$_2$O)Cl]

| | x | y | z | U(eq) |
|---|---|---|---|---|
| Fe | 5611(1) | 5994(1) | 1431(1) | 12(1) |
| Cl | 5721(1) | 6313(1) | 3323(1) | 23(1) |
| O(1) | 6240(1) | 4969(1) | 1746(1) | 16(1) |
| O(2) | 3899(1) | 5841(1) | 1033(1) | 16(1) |
| O(10) | 5654(2) | 5731(1) | −347(1) | 16(1) |
| O(20) | 11403(1) | 4475(1) | 4458(2) | 39(1) |
| O(21) | 10604(2) | 3415(1) | 4792(2) | 46(1) |
| O(30) | 6697(2) | 2840(1) | 2927(1) | 27(1) |
| O(31) | 5401(1) | 3735(1) | 2639(1) | 26(1) |
| O(50) | 536(2) | 7954(1) | −2286(2) | 57(1) |
| O(51) | 744(2) | 7158(1) | −1878(2) | 43(1) |
| O(60) | 568(1) | 5285(1) | 1097(1) | 24(1) |
| O(61) | 2174(1) | 4743(1) | 785(1) | 24(1) |
| N(1) | 7369(2) | 6307(1) | 1401(1) | 14(1) |
| N(2) | 5362(2) | 7081(1) | 769(1) | 25(1) |
| N(20) | 10561(2) | 4041(1) | 4342(2) | 27(1) |
| N(30) | 6426(2) | 3509(1) | 2808(1) | 18(1) |
| N(50) | 258(2) | 7414(1) | −1747(2) | 32(1) |
| N(60) | 1521(2) | 5296(1) | 753(1) | 17(1) |
| C(1) | 8288(2) | 5964(1) | 1919(2) | 16(1) |
| C(2) | 8280(20 | 5234(1) | 2495(2) | 16(1) |
| C(3) | 9352(2) | 4992(1) | 3137(2) | 18(1) |
| C(4) | 9436(2) | 4292(1) | 3654(2) | 19(1) |
| C(5) | 8478(2) | 3811(1) | 3530(2) | 19(1) |
| C(6) | 7408(2) | 4048(1) | 2899(2) | 15(1) |
| C(7) | 7247(2) | 4764(1) | 2365(2) | 14(1) |
| C(11) | 4414(2) | 7342(1) | 163(2) | 16(1) |
| C(12) | 3264(2) | 6959(1) | −58(2) | 16(1) |
| C(13) | 2336(2) | 7337(1) | −750(2) | 20(1) |
| C(14) | 1203(2) | 7039(1) | −940(2) | 22(1) |
| C(15) | 937(2) | 6381(1) | −425(2) | 19(1) |
| C(16) | 1857(2) | 5996(1) | 239(2) | 16(1) |
| C(17) | 3057(2) | 6241(1) | 432(2) | 14(1) |
| C(20) | 7479(2) | 7021(1) | 789(2) | 19(1) |
| C(21) | 6462(2) | 7529(1) | 979(2) | 19(1) |
| O(90) | 6466(2) | 4188(1) | 5129(1) | 32(1) |
| O(91) | 7541(2) | 4185(1) | 6843(2) | 36(1) |
| N(90) | 6810(2) | 4474(1) | 6086(2) | 22(1) |
| C(90) | 6277(2) | 5199(1) | 6336(2) | 26(1) |

[a] See Fig. 7 for atomic labeling scheme; atoms labeled (90) and (91) refer to the nitromethane of crystallization.
[b] U(eq) is defined as one third of the trace of the orthogonalized $U_{ij}$ tensor.

molecular hydrogen bonds between different complex molecules in the solid state.

## Acknowledgements

Parts of this work were supported by the U.S. Army Research Office; the U.S. Department of Energy, Morgantown Energy Technology Center; the Gas Research Institute, and the Sun Company. E.R.B. and M.W.G. thank NDSEF and NIH for graduate and postdoctoral fellowships, respectively. A.B. thanks the Alexander von Humboldt Foundation for a postdoctoral scholarship.

## References

[1] R.A. Sheldon (Ed.), Metalloporphyrins in Catalytic Oxidations (Marcel Dekker, New York, 1994), and references cited therein.
[2] P.E. Ellis and J.E. Lyons, Catal. Lett. 3 (1989) 389; Coord. Chem. Rev. 105 (1990) 181; J.E. Lyons and P.E. Ellis, Catal. Lett. 8 (1991) 45; in: Metalloporphyrins in Catalytic Oxidations, R.A. Sheldon (Ed.) (Marcel Dekker, New York, 1994) pp. 297–324; J.E. Lyons, P.E. Ellis and H.K. Myers, J. Catal. 155 (1995) 59.
[3] J.E. Lyons, P.E. Ellis and V.A. Durante, in: Structure-Activity and Selectivity Relationships in Heterogeneous Catalysis, R.K. Grasselli and A.W. Sleight (Eds.) (Elsevier, Amsterdam, 1991) pp. 99–116.
[4] M.W. Grinstaff, M.G. Hill, E.R. Birnbaum, W.P. Schaefer, J.A. Labinger and H.B. Gray, Inorg. Chem. 34 (1995) 4896.
[5] M.W. Grinstaff, M.G. Hill, J.A. Labinger and H.B. Gray, Science 264 (1994) 1311; T. Takeuchi, H.B. Gray and W.A. Goddard, J. Am. Chem. Soc. 116 (1994) 9730; E.R. Birnbaum, J.A. Labinger, J.E. Bercaw and H.B. Gray, Inorg. Chem. 34 (1995) 1751; J.A. Hodge, M.G. Hill and H.B. Gray, Inorg. Chem. 34 (1995) 809; E.R. Birnbaum, M.W. Grinstaff, J.A. Labinger and H.B. Gray, J. Mol. Catal. 104 (1995) L119.
[6] J.A. Labinger, Catal. Lett. (1994) 26, 95.
[7] A. Böttcher, M.W. Grinstaff, J.A. Labinger and H.B. Gray, J. Mol. Catal., in press.
[8] Ingold et al. and Que et al., J. Mol. Catal. A (1996), this issue.
[9] M.W. Grinstaff, M.G. Hill, J.A. Labinger and H.B. Gray, Science (1994) 264, 1311.
[10] J.E. Lyons, P.E. Ellis, H.K. Myers and R.W. Wagner, J. Catal. (1993) 141, 311.
[11] R.A. Sheldon and J.K. Kochi, Metal-Catalyzed Oxidations of Organic Compounds (Academic Press, New York, 1981) p. 344.
[12] K.T. Moore, I.T. Horváth and M.J. Therien, private communication.
[13] G.N. La Mar, G.R. Eaton, R.H. Holm and F.A. Walker, J. Am. Chem. Soc. 95 (1973) 63.
[14] M. Gerloch and F.E. Mabbs, J. Chem. Soc. A (1967) 1598.
[15] M. Gerloch, J. Lewis, F.E. Mabbs and J. Richards, Nature 212 (1966) 809.
[16] M. Gerloch and F.E. Mabbs, J. Chem. Soc. A (1967) 1900.
[17] M. Gerloch, J. Lewis, F.E. Mabbs and J. Richards, J. Chem. Soc. A (1968) 112.

[18] B.J. Kennedy, G. Brain, E. Horn, K.S. Murray and M.R. Snow, Inorg. Chem. 24 (1985) 1647.
[19] Y. Nishida, K. Kino and S. Kida, J. Chem. Soc., Dalton Trans. (1987) 1157.
[20] R.E. Marsh, W.P. Schaefer, J.A. Hodge, M.E. Hughes, H.B. Gray, J.E. Lyons and P.E. Ellis, Jr., Acta Crystallogr. C 49 (1993) 1339; W.P. Schaefer, J.A. Hodge, M.E. Hughes, H.B. Gray, J.E. Lyons, P.E. Ellis, Jr. and R.W. Wagner, Acta Crystallogr. C 49 (1993) 1342; L.M. Henling, W.P. Schaefer, J.A. Hodge, M.E. Hughes, H.B. Gray, J.E. Lyons and P.E. Ellis, Jr., Acta Crystallogr. C 49 (1993) 1743; E.R. Birnbaum, J.A. Hodge, M.G. Grinstaff, W.P. Schaefer, R.E. Marsh, L.M. Henling, J.A. Labinger, J.E. Bercaw and H.B. Gray, Inorg. Chem. 34 (1995) 3625.
[21] F. Corazza, C. Floriani and M. Zehnder, J. Chem. Soc., Dalton Trans. (1987) 709.
[22] X. Wang, W.T. Pennington, D.L. Ankers and J.C. Fanning, Polyhedron 17 (1992) 2253.
[23] D.T. Cromer and J.T. Waber, International Tables for X-Ray Crystallography, Vol. IV (Kynoch Press, Birmingham, 1974) pp. 99–101.
[24] D.T. Cromer, International Tables for X-Ray Crystallography, Vol. IV (Kynoch Press, Birmingham, 1974) pp. 149–151.
[25] D.J. Duchamp, in: Am. Crystallogr. Assoc. Meet., Bozeman, Montana (1964) paper B14, p. 29.
[26] G.M. Sheldrick, Acta Crystallogr. A 46 (1990) 467.
[27] G.M. Sheldrick, Program for Structure Refinement (University of Göttingen, Germany, 1993).
[28] XP/PC, Molecular Graphics Software, Siemens Analytical X-Ray Instruments.